FINAL GRADUATION PROJECT MONOGRAPH

The α-$\mathcal{F}$ Composite Distribution with Pointing Errors: Theory and Applications to RIS

Pedro Henrique Dornelas Almeida

Lucas Rabelo Andrade

Graduate Course in Communications Network Engineering

DEPARTMENT OF ELECTRICAL ENGINEERING

UNIVERSITY OF BRASÍLIA
FACULTY OF TECHNOLOGY

FINAL GRADUATION PROJECT MONOGRAPH

The α-$\mathcal{F}$ Composite Distribution with Pointing Errors: Theory and Applications to RIS

Pedro Henrique Dornelas Almeida

Lucas Rabelo Andrade

Final graduation project monograph submitted to the Department of Electrical Engineering as partial requirement for the degree of Bachelor in Communication Networks Engineering

Examining Board

Dr. Hugerles Sales Silva, EnE/UnB _____
Supervisor

Dr. Ugo Silva Dias, EnE/UnB _____
Co-supervisor

Dr. Francisco Assis de Oliveira Nascimento, EnE/UnB _____
Internal Examiner

Dr. Marcelo Menezes de Carvalho, EnE/UnB _____
Internal Examiner

CATALOG SHEET

ALMEIDA, PEDRO HENRIQUE DORNELAS
ANDRADE, LUCAS RABELO
The α-$\mathcal{F}$ Composite Distribution with Pointing Errors: Theory and Applications to RIS [Federal District] 2023.
24 p., 210 x 297 mm (ENE/FT/UnB, Bachelor, Communications Network Engineering, 2023).
Final graduation project monograph - University of Brasília, Faculty of Technology.
Department of Electrical Engineering

1. Telecommunications	2. Channel modeling
3. Reconfigurable intelligent surfaces	4. Performance metrics
I. ENE/FT/UnB	II. Title (series)

BIBLIOGRAPHICAL REFERENCE

ALMEIDA, P.H.D., ANDRADE, L.R. (2023). *The α-$\mathcal{F}$ Composite Distribution with Pointing Errors: Theory and Applications to RIS*. Final graduation project monograph, Department of Electrical Engineering, University of Brasília, Brasília, DF, 24 p.

ASSIGNMENT OF RIGHTS

Pedro Henrique Dornelas Almeida
Department of Electrical Engineering (ENE) - FT
University of Brasília (UnB)
Darcy Ribeiro Campus
CEP: 70919-970 - Brasília-DF - Brasil

Lucas Rabelo Andrade
Department of Electrical Engineering (ENE) - FT
University of Brasília (UnB)
Darcy Ribeiro Campus
CEP: 70919-970 - Brasília-DF - Brasil

RESUMO

A distribuição de desvanecimento composto α-$\mathcal{F}$ com erros de apontamento é investigada neste estudo. Novas expressões para a função de densidade de probabilidade e função de distribuição cumulativa do envelope/relação sinal-ruído (SNR) instantânea, momentos de ordem superior e a função geradora de momentos da SNR instantânea também são derivadas. Com base nas estatísticas mencionadas anteriormente, expressões para a probabilidade de interrupção, probabilidade de erro de símbolo e capacidade ergódica do canal são obtidas. Uma análise assintótica também é fornecida. Além disso, uma aplicação do modelo α-$\mathcal{F}$ com erros de apontamento em um sistema sem fio emergente, chamado de superfícies inteligentes reconfiguráveis (RIS) é demonstrado. Várias curvas, corroboradas por simulações realizadas com o método de Monte-Carlo, são apresentadas para diferentes valores de parâmetros que caracterizam o canal e o erro de apontamento.

Palavras-chave: distribuição de desvanecimento composto α-$\mathcal{F}$, RIS, métricas de desempenho, erros de apontamento.

ABSTRACT

The α-$\mathcal{F}$ composite fading distribution with pointing errors is investigated in this study. New expressions for the probability density function and cumulative distribution function of the envelope/instantaneous signal-to-noise ratio (SNR), higher-order moments, and moment generating function of the instantaneous SNR are derived. Based on the aforementioned statistics, expressions for the outage probability, symbol error probability, and ergodic channel capacity are obtained. An asymptotic analysis is also provided. Furthermore, an application of the α-$\mathcal{F}$ model with pointing errors in a wireless emerging system, namely reconfigurable intelligent surfaces (RIS), is shown. Several curves, corroborated by Monte-Carlo simulations, are presented for different values that characterize the channel and pointing errors parameters.

Keywords: α-$\mathcal{F}$ composite fading distribution, RIS, performance metrics, pointing errors.

SUMMARY

FIGURES LIST

TABLES LIST

List of Abbreviations and Acronyms

Acronyms

PDF	*Probability Density Function*
CDF	*Cumulative Distribution Function*
SNR	*Signal-to-Noise Ratio*
MGF	*Moment-Generating Function*
OP	*Outage Probability*
SEP	*Symbol Error Probability*
BEP	*Bit Error Probability*
RIS	*Reconfigurable Intelligent Surfaces*
FSO	*Free-Space Optical Communication*
LoS	*Line-of-Sight*
NLoS	*Non-Line-of- Sight*

1 INTRODUCTION

This chapter presents the state-of-the-art of the topic in study; the main contributions obtained by us as well as the organization of this work.

1.1 OVERVIEW

Nowadays, the fifth generation (5G) of mobile communications is characterized as a promising and essential technology to meet the high demands and requirements of new vertical use cases. In order to support it, terahertz (THz) band frequencies have attracted the interest of several researchers around the world, mainly due to the broader available spectrum, higher throughputs, and for supporting a greater number of simultaneous users [1]. As disadvantages, THz bands present high atmospheric attenuation, which can be compensated by the system with the use of high-directional antenna arrays. However, this causes misalignment between the transmitting and receiving antennas, which results in pointing errors [2]. Despite pointing errors being an important factor to be considered in many studies, it should be mentioned that including them in expressions that can be evaluated the performance of communication systems makes the analysis more difficult and, therefore, many authors ignore this effect.

Recent works are described in the literature where the misalignment is adopted in different contexts, such as single-hop [2, 3], dual-hop [4], multiple-input multiple-output [5] and non-orthogonal multiple access-THz [6] transmission systems, free space optics (FSO) [7] and reconfigurable intelligent surfaces (RIS) [8], for example. In [9], an analytical framework is presented in order to evaluate the joint effect of misalignment and hardware imperfections in the presence of multipath fading, modeled by the α-μ distribution, in a THz wireless fiber extenders system. The α-μ distribution is also considered in other important papers, such as in [3], where a performance analysis of THz systems in random fog conditions with misalignment is performed, and in [8], in which expressions are derived for many statistics and metrics under RIS-aided THz wireless systems with pointing errors. In [7], an analysis is fulfilled about FSO communications over Fisher-Snedecor $\mathcal{F}$ turbulence channels with pointing errors. In the mentioned analysis, expressions for the probability density function (PDF) and cumulative distribution function (CDF) of the instantaneous signal-to-noise ratio (SNR) are derived and employed to obtain novel closed-form expressions for metrics such as outage probability (OP), average bit error probability (BEP) and average ergodic capacity.

Experimental works concerning THz wireless links are also presented in the literature, such as [10], [11]. In [10], fitting results are presented of α-μ, Nakagami-m, Rice, and log-normal distributions to the small-scale fading of THz wireless channel measurements, where the α-μ provided the best adherence. Additionally, the performance of the ergodic capacity is assessed. In [11], a measurement campaign is also conducted by the same authors of [10], considering various line-of-sight (LoS) and non-LoS links, in which α-μ distribution is fitted to experimental THz channel gain measurements. In the above-mentioned papers, shadowing is not considered. However, as reported in [12], shadowing is an important factor to be

analyzed in THz systems.

In this work, a study of the α-$\mathcal{F}$ fading distribution with pointing errors is performed, in which new expressions for relevant statistics and metrics are derived. Based on the literature described, there is no work that addresses the α-$\mathcal{F}$ distribution with pointing errors. In our work, the α-$\mathcal{F}$ model is considered since [13]: (i) it is simple, characterized in terms of physical parameters, and generalist, encompassing other distributions as particular cases; (ii) it characterizes small and large-scale fading, as well as the non-linearity of the communication channel; (iii) is supported by experimental results and adopted in many works under different scenarios. It should be mentioned that the advantages offered by the α-$\mathcal{F}$ and pointing errors distributions make the model presented in this work more realistic, with a greater degree of freedom than other distributions, such as α-$\mathcal{F}$ and Fisher-Snedecor.

1.2 CONTRIBUTIONS OF THIS WORK

The main contributions of this work are:

- A study about the α-$\mathcal{F}$ with pointing errors is performed, in which new closed-form expressions are derived for the PDFs and CDFs, higher-order moments, and moment generating function (MGF) of the instantaneous SNR;
- New expressions are derived for OP, symbol error probability (SEP), and channel capacity;
- Asymptotic expressions are also deduced in order to provide insights into the effect of the channel and pointing errors parameters on the system performance;
- An application is described of the α-$\mathcal{F}$ model with pointing errors in a RIS-assisted wireless emerging system.

1.3 ORGANIZATION OF THIS WORK

The remaining of the study is organized as follows: Chapter 2 describes the system and channel models adopted. In Chapter 3, statistics are derived for the α-$\mathcal{F}$ composite fading distribution with pointing errors. For the aforementioned distribution, metrics and asymptotic metrics are presented in Chapters 4 and 5, respectively. Chapter 6 describes a RIS assisted scenario with pointing errors. Chapter 7 shows the numerical results and discussions. Chapter 8 brings the conclusions of the study.

2 SYSTEM AND CHANNEL MODELS

In this chapter, the system and channel models considered in our work are presented.

2.1 SYSTEM MODEL

The received signal y can be written as

$$y = h_{\text{l}} h_{\text{f}} h_{\text{p}} x + n, \tag{2.1}$$

in which x is the transmitted signal, n is the additive white Gaussian noise, h_{f} denotes the composite fading channel, h_{p} represents the misalignment component, and h_{l} is the path loss, that is constant for a given weather condition and link distance. For THz systems, $h_{\text{l}} = h_{\text{fl}} h_{\text{al}}$, where h_{fl} models the propagation gain and h_{al} characterizes the molecular absorption gain. More details about the path-gain coefficient can be found in [2].

2.2 FADING MODEL

The fading channel is characterized in our study by the α-$\mathcal{F}$ composite distribution, that is derived from the Fisher-Snedecor $\mathcal{F}$ model. The α-$\mathcal{F}$ characterizes jointly the small and large-scale fading, as well as the non-linearity of the propagation medium.

The envelope PDF of the α-$\mathcal{F}$ composite distribution is given by [13]

$$f_{H_{\text{f}}}(h_{\text{f}}) = \frac{\alpha h_{\text{f}}^{\alpha\mu-1}}{\text{B}(\mu, m)} \left(\frac{\hat{r}^{\alpha}}{\Psi}\right)^{m} \left(h_{\text{f}}^{\alpha} + \frac{\hat{r}^{\alpha}}{\Psi}\right)^{-(\mu+m)}, \tag{2.2}$$

where $\Psi = \mu/(m-1)$, $\hat{r} = \sqrt[\alpha]{\mathbb{E}[H_{\text{f}}^{\alpha}]}$ denotes the α-root mean value, α characterizes the non-linearity of the propagation medium, μ represents the number of multipath clusters, m is the shadowing parameter and $\text{B}(\cdot,\cdot)$ is the Beta function [14, Eq. (06.18.02.0001.01)]. From the α-$\mathcal{F}$ model, the α-μ and Fisher-Snedecor $\mathcal{F}$ channels can be obtained by making $m \to \infty$ and $\alpha = 2$, respectively.

2.3 POINTING ERROR MODEL

The pointing error PDF impairment is given by [7, Eq. (7)]

$$f_{H_{\text{p}}}(h_{\text{p}}) = z^2 A_0^{-z^2} h_{\text{p}}^{z^2-1}, \;\; 0 \leq h_{\text{p}} \leq A_0, \tag{2.3}$$

in which A_0 is the fraction of the collected power and $z = \omega_{\text{eq}}/\sigma$ is the ratio between the equivalent beam radius at the receiver and the pointing error displacement standard deviation [15]. For $z \to \infty$, it should be mentioned that case of the non-pointing error is assumed.

The pointing errors, represented by the parameter z in (2.3), concerns the misalignment that occurs between the transmitting and the receiving antennas, being caused mainly by physical imperfections in the transceivers. It is considerable mainly in systems that require high-directivity, such as in THz communication systems.

3 THE α-$\mathcal{F}$ COMPOSITE FADING DISTRIBUTION WITH POINTING ERRORS

In this chapter, several statistics for the α-$\mathcal{F}$ composite fading model with pointing errors are derived.

3.1 PDF AND CDF OF THE ENVELOPE

Proposition 3.1.1. *Let μ, m, $\hat{r}^{\alpha}$, z, A_0, h_l, $h \in \mathbb{R}^{+}$ and $m > 1$. The PDF and the CDF of the envelope $H = h_l H_f H_p$, for the α-$\mathcal{F}$ composite fading model with pointing errors, can be obtained, respectively, as*

$$f_H(h) = \frac{z^2}{h\Gamma(\mu)\Gamma(m)} \mathrm{G}_{2,2}^{2,1}\left[\Psi\left(\frac{h}{\hat{r}h_l A_0}\right)^{\alpha} \middle| \begin{matrix} 1-m, z^2/\alpha+1 \\ \mu, z^2/\alpha \end{matrix}\right] \tag{3.1}$$

and

$$F_H(h) = \frac{z^2}{\alpha\Gamma(\mu)\Gamma(m)} \mathrm{G}_{3,3}^{2,2}\left[\Psi\left(\frac{h}{\hat{r}h_l A_0}\right)^{\alpha} \middle| \begin{matrix} 1-m, 1, z^2/\alpha+1 \\ \mu, z^2/\alpha, 0 \end{matrix}\right] \tag{3.2}$$

where $\Gamma(\cdot)$ is the Gamma function [14, Eq. (06.05.02.0001.01)] and $\mathrm{G}[\cdot]$ is the Meijer G-function[1] [16, Eq. (9.301)].

Proof. The PDF of $H = h_{\mathrm{l}} H_{\mathrm{f}} H_{\mathrm{p}}$, denoted by $f_H(h)$, can be derived by means of

$$f_H(h) = \frac{1}{h_{\mathrm{l}}} \int_0^{\infty} \frac{1}{v} f_{H_{\mathrm{f}}}\Big(\frac{h}{h_{\mathrm{l}} v}\Big) f_{H_{\mathrm{p}}}(v) \mathrm{d}v. \tag{3.3}$$

Substituting (2.2) and (2.3) in the expression of $f_H(h)$, performing the change of variable $t = v^{-\alpha}$ and using [16, Eq. (3.194.2)], $f_H(h)$ can be written after simplifications as

$$f_H(h) = \frac{\alpha z^2}{h\mathrm{B}(\mu, m)(\alpha m + z^2)} \left(\frac{A_0^{\alpha}\hat{r}^{\alpha}}{\Psi}\right)^{m} \left(\frac{h_{\mathrm{l}}}{h}\right)^{\alpha m} {}_2\mathrm{F}_1\Big[\mu + m, m + \frac{z^2}{\alpha},\ m + \frac{z^2}{\alpha} + 1;\ -\xi\Big], \tag{3.4}$$

in which $\xi = (m-1)\hat{r}^{\alpha} h_{\mathrm{l}}^{\alpha} A_0^{\alpha}/(\mu h^{\alpha})$ and ${}_2\mathrm{F}_1[\cdot,\cdot,\cdot;\cdot]$ is the Gauss hypergeometric function [16, Eq. (9.100)]. In sequence, employing [17, Eq. (8.4.49.14)] and [18, Eq. (9.31.5)] and performing with some algebraic manipulations, (3.1) is obtained.

The CDF of H, $F_H(h)$, can be derived integrating (3.1), i.e,

$$F_H(h) = \frac{z^2}{\Gamma(\mu)\Gamma(m)} \int_0^{h} \frac{1}{x} \mathrm{G}_{2,2}^{2,1}\left[\Psi\left(\frac{x}{\hat{r}h_{\mathrm{l}} A_0}\right)^{\alpha} \middle| \begin{matrix} 1-m, z^2/\alpha+1 \\ \mu, z^2/\alpha \end{matrix}\right] \mathrm{d}x. \tag{3.5}$$

[1] The representations for the Meijer-G, Fox H-function and multivariate Fox H-function in terms of the Mellin-Barnes integrals are presented in Appendix.

Expressing the Meijer G-function of (3.5) in terms of the Mellin-Barnes integral, the innermost integral in the variable x is of the power-type and can be solved. In addition, using $\Gamma(x+1) = x\Gamma(x)$ and the definition of the Meijer G-function, (3.2) is derived. Hence, the proof is complete.

□

3.2 PDF AND CDF OF THE INSTANTANEOUS SNR

Proposition 3.2.1. *For μ, m, $\bar{\gamma}$, z, A_0, h_l, $\gamma \in \mathbb{R}^+$ and $m > 1$, the PDF of the instantaneous SNR Γ, in the presence of α-$\mathcal{F}$ composite fading with pointing errors, is given by*

$$f_\Gamma(\gamma) = \frac{z^2}{2\gamma\Gamma(\mu)\Gamma(m)} \mathrm{G}_{2,2}^{2,1}\left[\Psi\left(\frac{z\sqrt{\gamma}}{\sqrt{\bar{\gamma}(z^2+2)}}\right)^{\alpha} \middle| \begin{matrix} 1-m, z^2/\alpha+1 \\ \mu, z^2/\alpha \end{matrix}\right], \tag{3.6}$$

in which $\bar{\gamma}$ is the average SNR. In turn, the CDF $F_\Gamma(\gamma)$ is written as

$$F_\Gamma(\gamma) = \frac{z^2}{\alpha\Gamma(\mu)\Gamma(m)} \mathrm{G}_{3,3}^{2,2}\left[\Psi\left(\frac{z\sqrt{\gamma}}{\sqrt{\bar{\gamma}(z^2+2)}}\right)^{\alpha} \middle| \begin{matrix} 1-m, 1, z^2/\alpha+1 \\ \mu, z^2/\alpha, 0 \end{matrix}\right]. \tag{3.7}$$

Proof. Making $\Gamma = H^2$, the PDF of the instantaneous SNR can be obtained by means of

$$f_\Gamma(\gamma) = \frac{1}{2\sqrt{\gamma}} f_H(\sqrt{\gamma}). \tag{3.8}$$

Using (3.1), (3.6) is easily deduced. Furthermore, $F_\Gamma(\gamma)$ is derived from (3.2), since $F(\gamma) = F_H(\sqrt{h})$. The result for $F_\Gamma(\gamma)$ is presented in (3.7) and complete the proof. □

3.3 HIGHER-ORDER MOMENTS OF THE INSTANTANEOUS SNR

Proposition 3.3.1. *For μ, m, $\bar{\gamma}$, z, A_0, $h_l \in \mathbb{R}^+$ and $k \in \mathbb{N}^+$, the higher-order moments of the instantaneous SNR over the α-$\mathcal{F}$ composite fading model with pointing errors, is obtained as*

$$\mathbb{E}[\gamma^k] = \frac{z^2\Gamma(\mu+\frac{2k}{\alpha})\Gamma(m-\frac{2k}{\alpha})}{(z^2+2k)\Gamma(\mu)\Gamma(m)} \left(\frac{\sqrt{\bar{\gamma}(z^2+2)}}{z\Psi^{\frac{1}{\alpha}}}\right)^{2k}, \tag{3.9}$$

which is valid for $m > 2k/\alpha$.

Proof. The higher-order moments of the instantaneous SNR, $\mathbb{E}[\gamma^k]$, is calculated as

$$\mathbb{E}[\gamma^k] = \int_0^\infty \gamma^k f_\Gamma(\gamma) \mathrm{d}\gamma. \tag{3.10}$$

Substituting (3.6),

$$\mathbb{E}[\gamma^k] = \frac{z^2}{2\Gamma(\mu)\Gamma(m)} \int_0^\infty \frac{\gamma^k}{\gamma} \mathrm{G}_{2,2}^{2,1}\left[\Psi \left(\frac{z\sqrt{\gamma}}{\sqrt{\bar{\gamma}(z^2+2)}} \right)^\alpha \middle| \begin{matrix} 1-m, z^2/\alpha+1 \\ \mu, z^2/\alpha \end{matrix} \right] \mathrm{d}\gamma. \tag{3.11}$$

Performing the variable change $x = \gamma^{\alpha/2}$, using [16, Eq. (7.811.4)] and making some algebraic manipulations, (3.9) is derived, that complete the proof. □

3.4 MGF OF THE INSTANTANEOUS SNR

Proposition 3.4.1. *Let μ, m, $\bar{\gamma}$, z, A_0, h_l, $s \in \mathbb{R}^+$ and $m > 1$. The MGF of the instantaneous SNR over the α-$\mathcal{F}$ composite fading model with pointing errors is given by*

$$\mathrm{M}_\Gamma(s) = \frac{z^2}{2\Gamma(\mu)\Gamma(m)} \mathrm{H}_{3,3}^{2,2}\left[\left(\frac{z\Psi^{\frac{1}{\alpha}}}{\sqrt{s\bar{\gamma}(z^2+2)}} \right)^\alpha \middle| \begin{matrix} (1-m,1),(1,\frac{\alpha}{2}),(\frac{z^2}{\alpha}+1,1) \\ (\mu,1),(\frac{z^2}{\alpha},1) \end{matrix} \right], \tag{3.12}$$

with $\mathrm{H}[\cdot]$ denoting the Fox H-function [18, Eq. (1.2)].

Proof. The MGF is defined as

$$\mathrm{M}_\Gamma(s) = \int_0^\infty f_\Gamma(\gamma) \exp(-s\gamma) \mathrm{d}\gamma. \tag{3.13}$$

Replacing (3.6), using [14, 07.34.26.0008.01], [14, 01.03.26.0004.01] and [19, Eq. (2.8.4)], (3.12) can be obtained after simplifications. Hence, the proof is complete. □

3.5 SPECIAL CASES

The α-$\mathcal{F}$ composite distribution with pointing errors generalizes various other models presented in the literature, by properly selecting the fading parameters α, μ and m with specific values. Table 3.1 summarizes the commom fading channels extracted from the α-$\mathcal{F}$ with pointing errors.

Table 3.1: Special cases.

Fading Channels with Pointing Errors	Parameters
α-μ	$\alpha = \alpha$, $\mu = \mu$, $z = z$, $m \to \infty$
Fisher-Snedecor $\mathcal{F}$	$\alpha = 2$, $\mu = \mu$, $z = z$, $m = m_s$
Nakagami-m	$\alpha = 2$, $\mu = m$, $z = z$, $m \to \infty$
Weibull	$\alpha = \alpha$, $\mu = 1$, $z = z$, $m \to \infty$
Rayleigh	$\alpha = 2$, $\mu = 1$, $z = z$, $m \to \infty$
One-Gaussian	$\alpha = 2$, $\mu = 0.5$, $z = z$, $m \to \infty$
Nakagami-$\mathcal{F}$	$\alpha = 2$, $\mu = m$, $z = z$, $m = m_s$
Weibull-$\mathcal{F}$	$\alpha = \alpha$, $\mu = 1$, $z = z$, $m = m_s$
Rayleigh-$\mathcal{F}$	$\alpha = 2$, $\mu = 1$, $z = z$, $m = m_s$
One-Gaussian-$\mathcal{F}$	$\alpha = 2$, $\mu = 0.5$, $z = z$, $m = m_s$

4 PERFORMANCE ANALYSIS

In this chapter, metrics such as OP, BEP, ergodic channel capacity as well the asymptotics ones are presented.

4.1 METRICS PERFORMANCE

4.1.1 Outage Probability

The OP, $P_{\rm out}$, is defined as the point in which the SNR at the output of the receiver falls below a threshold $\gamma_{\rm th}$. Mathematically, by using (3.7), $P_{\rm out} = F_{\Gamma}(\gamma_{\rm th})$.

4.1.2 Symbol Error Probability

The average SEP, $P_{\rm sym}$, can be evaluated as [20, Eq. (7)]

$$P_{\rm sym} = \frac{\theta}{2\sqrt{2\pi}} \int_0^{\infty} \frac{1}{\sqrt{\gamma}} \exp\left(-\gamma/2\right) F_{\gamma}\left(\frac{\gamma}{\phi}\right) {\rm d}\gamma, \tag{4.1}$$

in which the parameters θ and ϕ depend on the type of modulation.

Substituting (3.7) into (4.1), using [14, 07.34.26.0008.01],[14, 01.03.26.0004.01] and [19, Eq. (2.8.4)], after simplifications, the SEP is given by

$$P_{\rm sym} = \frac{\theta z^2}{2\sqrt{\pi}\alpha\Gamma(\mu)\Gamma(m)} {\rm H}_{4,3}^{2,3}\left[\Psi \left(\frac{z\sqrt{2}}{\sqrt{\phi\bar{\gamma}(z^2+2)}} \right)^{\alpha} \middle| \begin{matrix} (1-m,1),(1,1),(1/2,\frac{\alpha}{2}),(\frac{z^2}{\alpha}+1,1) \\ (\mu,1),(\frac{z^2}{\alpha},1),(0,1) \end{matrix} \right]. \tag{4.2}$$

4.1.3 Channel Capacity

The channel capacity, in bps/Hz, is calculated as

$$C_{\rm erg} = \frac{1}{\ln(2)} \int_0^{\infty} f_{\Gamma}(\gamma) \ln(1+\gamma) {\rm d}\gamma. \tag{4.3}$$

Replacing (3.6) in the expression of $C_{\rm erg}$ and using [14, 01.04.26.0003.01], [14, 07.34.26.0008.01], [14, 01.03.26.0004.01] and [19, Eq. (2.8.4)], the channel capacity can be written as

$$C_{\rm erg} = \frac{z^2}{2\ln(2)\Gamma(\mu)\Gamma(m)} {\rm H}_{4,4}^{4,2}\left[\frac{z^{\alpha}\Psi}{\left(\bar{\gamma}(z^2+2)\right)^{\alpha/2}} \middle| \begin{matrix} (1-m,1),(0,\frac{\alpha}{2}),(1,\frac{\alpha}{2}),(\frac{z^2}{\alpha}+1,1) \\ (\mu,1),(\frac{z^2}{\alpha},1),(0,\frac{\alpha}{2}),(0,\frac{\alpha}{2}) \end{matrix} \right]. \tag{4.4}$$

4.2 ASYMPTOTIC ANALYSIS

4.2.1 Asymptotic Outage Probability

For $\bar{\gamma} \to \infty$, the asymptotic OP can be derived by means of (3.7), using [14, 07.34.26.0008.01] and [19, Theorem 1.11], in which only the dominant term is considered. After simplifications, $P_{\rm out}^{\infty}$ is written as

$$P_{\rm out}^{\infty} = \begin{cases} \frac{z^2 \Psi^{\mu}}{(z^2\mu - \alpha\mu^2)\mathrm{B}(\mu,m)} \left(\frac{\sqrt{\bar{\gamma}(z^2+2)}}{z\sqrt{\gamma_{\rm th}}} \right)^{-\alpha\mu} & , \alpha\mu < z^2 \\ \frac{\Gamma(\mu - \frac{z^2}{\alpha})\Gamma(m + \frac{z^2}{\alpha})}{\Gamma(\mu)\Gamma(m)\Psi^{-\frac{z^2}{\alpha}}} \left(\frac{\sqrt{\bar{\gamma}(z^2+2)}}{z\sqrt{\gamma_{\rm th}}} \right)^{-z^2} & , \alpha\mu > z^2 \end{cases}. \tag{4.5}$$

In high SNRs values, $P_{\rm out}^{\infty} \sim \bar{\gamma}^{-G_{\rm d}}$, where $G_{\rm d}$ is the diversity order/gain. From (4.5), it is noted that

$$G_{\rm d} \;=\; \min(\alpha\mu/2, z^2/2). \tag{4.6}$$

That is, the diversity order depends on the fading and pointing errors parameters.

4.2.2 Asymptotic Symbol Error Probability

For $\bar{\gamma} \to \infty$, the asymptotic SEP can be deduced applying [19, Theorem 1.11] in (4.2), as given by

$$P_{\rm sym}^{\infty} = \begin{cases} \frac{\theta z^2 \Gamma(\frac{\alpha\mu+1}{2})\Psi^{\mu}}{2\sqrt{\pi}\mu(z^2 - \alpha\mu)\mathrm{B}(\mu,m)} \left(\frac{\sqrt{\bar{\gamma}\phi(z^2+2)}}{z\sqrt{2}} \right)^{-\alpha\mu} & , \alpha\mu < z^2 \\ \frac{\theta\Gamma(\mu - \frac{z^2}{\alpha})\Gamma(m + \frac{z^2}{\alpha})\Gamma(\frac{1+z^2}{2})}{2\sqrt{\pi}\Gamma(\mu)\Gamma(m)\Psi^{-\frac{z^2}{\alpha}}} \left(\frac{\sqrt{\bar{\gamma}\phi(z^2+2)}}{z\sqrt{2}} \right)^{-z^2} & , \alpha\mu > z^2 \end{cases} \tag{4.7}$$

after some algebraic manipulations. In (4.7), if only the dominant term is considered then $G_{\rm d}$ is equal to (4.6).

4.2.3 Asymptotic Ergodic Capacity

The asymptotic ergodic capacity at high SNR values is given by [21]

$$C_{\rm erg}^{\infty} = \log_2(\bar{\gamma}) + \log_2(e) \frac{\partial}{\partial n} \frac{\mathbb{E}[\gamma^n]}{\bar{\gamma}^n} \bigg|_{n=0}, \tag{4.8}$$

in which $\partial/\partial n$ is the first derivative operator. Replacing (3.9) in (4.8) and proceeding with simplifications,

$$C_{\rm erg}^{\infty} = \log_2(\bar{\gamma}) + 2\log_2(e) \left[\frac{\psi(\mu)}{\alpha} - \frac{\psi(m)}{\alpha} - \frac{1}{z^2} + \ln\left(\frac{\sqrt{z^2+2}}{z} \left(\frac{1}{\Psi} \right)^{1/\alpha} \right) \right], \tag{4.9}$$

with $\psi(x) = \Gamma'(x)/\Gamma(x)$ is the digamma function [16, Eq. (8.36)].

5 RIS-AIDED WIRELESS SYSTEM OVER α-$\mathcal{F}$ FADING WITH POINTING ERRORS

In this chapter, a RIS-aided system over α-$\mathcal{F}$ fading with pointing errors is considered, that is a new and emerging system. For the mentioned wireless scenario, the system model as well as some metrics in order to evaluate the performance are presented in this chapter.

5.1 SYSTEM MODEL

A RIS consists of a surface composed of several reflecting elements with the ability to change the electromagnetic properties of a received wave. RIS can establish a virtual channel between the transmitter and the receiver in order to assist the communication. Thus, finding applications in scenarios where there is a strong blockage in a LoS component between receiver and transmitter. RIS is also important in high frequency scenarios such as THz, where the path loss is very high.

In this application, the RIS is composed of L elements and the received signal is given by

$$y = \sum_{i=1}^{L} h_{i,1} h_{i,2} x + w, \tag{5.1}$$

where x is the transmitted signal, w is the zero-mean_σ^2-variance additive white Gaussian noise and $h_{i,1}$ and $h_{i,2}$ are the fading gains between the source and the i-th RIS element and between the i-th RIS element and the destination, respectively. Here, we assume that the phases of $h_{i,1}$ and $h_{i,2}$ are known and can be perfectly compensated at the RIS. This assumption of perfect channel state information has been widely used in the literature to maximize the received SNR [22, 23, 24].

5.2 PDF, CDF AND MGF OF THE INSTANTANEOUS SNR

Proposition 5.2.1. *The PDF, CDF and MGF of the instantaneous SNR Γ, under a sum of double α-$\mathcal{F}$ random variates with pointing errors, are given respectively by*

$$f_{\Gamma}(\gamma) = \frac{1}{2\gamma} \left[\prod_{i=1}^{L} \prod_{j=1}^{2} \frac{z_{i,j}^2}{\alpha_{i,j} \Gamma(\mu_{i,j}) \Gamma(m_{i,j})} \right] \times \mathrm{H}_{0,1:[5,4]_{i=1:L}}^{0,0:[4,3]_{i=1:L}} \left[\begin{array}{c|c|c} \Xi_1 \sqrt{\gamma} & - & [(1,1), \mathcal{A}_{i,1}, \mathcal{A}_{i,2}, \mathcal{B}_{i,1}, \mathcal{B}_{i,2}]_{i=1:L} \\ \vdots & & \\ \Xi_L \sqrt{\gamma} & \epsilon_1 & [\mathcal{C}_{i,1}, \mathcal{C}_{i,2}, \mathcal{D}_{i,1}, \mathcal{D}_{i,2}]_{i=1:L} \end{array} \right], \tag{5.2}$$

$$F_{\Gamma}(\gamma)=\frac{1}{2}\left[\prod_{i=1}^{L}\prod_{j=1}^{2}\frac{z_{i,j}^{2}}{\alpha_{i,j}\Gamma(\mu_{i,j})\Gamma(m_{i,j})}\right]$$
$$\times \mathrm{H}_{1,2:[5,4]_{i=1:L}}^{0,1:[4,3]_{i=1:L}}\left[\begin{array}{c|c|c}\Xi_1\sqrt{\gamma} & & \\ \vdots & \epsilon_3 & [(1,1),\mathcal{A}_{i,1},\mathcal{A}_{i,2},\mathcal{B}_{i,1},\mathcal{B}_{i,2}]_{i=1:L} \\ \Xi_L\sqrt{\gamma} & \epsilon_1,\epsilon_2 & [\mathcal{C}_{i,1},\mathcal{C}_{i,2},\mathcal{D}_{i,1},\mathcal{D}_{i,2}]_{i=1:L}\end{array}\right] \tag{5.3}$$

and

$$\mathrm{M}_{\Gamma}(s)=\frac{1}{2}\left[\prod_{i=1}^{L}\prod_{j=1}^{2}\frac{z_{i,j}^{2}}{\alpha_{i,j}\Gamma(\mu_{i,j})\Gamma(m_{i,j})}\right]$$
$$\times \mathrm{H}_{1,1:[5,4]_{i=1:L}}^{0,1:[4,3]_{i=1:L}}\left[\begin{array}{c|c|c}\frac{\Xi_1}{(-s)^{\frac{1}{2}}} & & \\ \vdots & \epsilon_3 & [(1,1),\mathcal{A}_{i,1},\mathcal{A}_{i,2},\mathcal{B}_{i,1},\mathcal{B}_{i,2}]_{i=1:L} \\ \frac{\Xi_L}{(-s)^{\frac{1}{2}}} & \epsilon_1 & [\mathcal{C}_{i,1},\mathcal{C}_{i,2},\mathcal{D}_{i,1},\mathcal{D}_{i,2}]_{i=1:L}\end{array}\right], \tag{5.4}$$

in which $\epsilon_1=(1;\{1\}_{i=1:L})$, $\epsilon_2=\left(0;\{\frac{1}{2}\}_{i=1:L}\right)$, $\epsilon_3=\left(1;\{\frac{1}{2}\}_{i=1:L}\right)$, $\mathcal{A}_{i,j}=(1-m_{i,j},1/\alpha_{i,j})$, $\mathcal{B}_{i,j}=\left(\frac{z_{i,j}^2}{\alpha_{i,j}}+1,1/\alpha_{i,j}\right)$, $\mathcal{C}_{i,j}=(\mu_{i,j},1/\alpha_{i,j})$, $\mathcal{D}_{i,j}=\left(\frac{z_{i,j}^2}{\alpha_{i,j}},1/\alpha_{i,j}\right)$ *and*

$$\Xi_i=\prod_{j=1}^{2}\frac{\Psi_{i,j}^{1/\alpha_{i,j}}}{\sqrt{\bar{\gamma}_{i,j}(z_{i,j}^2+2)}}. \tag{5.5}$$

Proof. Let $X=H_1H_2$, where $f_{H_j}(t)$, with $j=1,2$, is given by (3.1). The Mellin transform of $f_{H_j}(t)$, denoted by $\mathcal{M}[f_{H_j}(t)]$, can derived using [18, Eq. (2.9)] and making the variable change $y=t^{\alpha_j}$. After simplifications,

$$\mathcal{M}[f_{H_j}(t)]=\frac{z_j^2}{\alpha_j\Gamma(\mu_j)\Gamma(m_j)}\left[\frac{\Psi_j}{\left(\hat{r}_j h_{l_j}A_{0_j}\right)^{\alpha_j}}\right]^{\frac{(1-s)}{\alpha_j}}$$
$$\times\frac{\Gamma\left(\mu_j+\frac{(s-1)}{\alpha_j}\right)\Gamma\left(\frac{z_j^2}{\alpha_j}+\frac{(s-1)}{\alpha_j}\right)\Gamma\left(1-(1-m_j)-\frac{(s-1)}{\alpha_j}\right)}{\Gamma\left(\frac{z_j^2}{\alpha_j}+1+\frac{(s-1)}{\alpha_j}\right)},\ j=1,2. \tag{5.6}$$

According to [25, Eq. (3.5)], $\mathcal{M}[f_X(x)]=\mathcal{M}[f_{H_1}(t)]\mathcal{M}[f_{H_2}(v)]$, and the PDF of X can be deduced using [25, Eq. (3.2)]

$$f_X(x)=\frac{1}{2\pi j}\int_{\mathcal{C}}x^{-s}\mathcal{M}[f_X(x)]\mathrm{d}s, \tag{5.7}$$

that is written after simplifications as

$$f_X(x)=\prod_{j=1}^{2}\frac{z_j^2\Psi_j^{1/\alpha_j}}{\alpha_j\Gamma(\mu_j)\Gamma(m_j)\hat{r}_j h_{l_j}A_{0_j}}\mathrm{H}_{4,4}^{4,2}\left[x\prod_{j=1}^{2}\frac{\Psi_j^{1/\alpha_j}}{\hat{r}_j h_{l_j}A_{0_j}}\middle|\begin{array}{c}\Phi_1,\Phi_2,\Theta_1,\Theta_2\\ \Upsilon_1,\Upsilon_2,\Omega_1,\Omega_2\end{array}\right], \tag{5.8}$$

in which $\Phi_j = \left(1 - m_j - \frac{1}{\alpha_j}, \frac{1}{\alpha_j}\right)$, $\Upsilon_j = \left(\mu_j - \frac{1}{\alpha_j}, \frac{1}{\alpha_j}\right)$, $\Theta_j = \left(\frac{z_j^2-1}{\alpha_j} + 1, \frac{1}{\alpha_j}\right)$ and $\Omega_j = \left(\frac{z_j^2-1}{\alpha_j}, \frac{1}{\alpha_j}\right)$.

In turn, the MGF of X can be calculated as

$$\mathrm{M}_X(t) = \int_0^\infty f_X(x) \exp(-tx) dx \Big|_{(-t)}. \tag{5.9}$$

Substituting (5.8) in (5.9), using [16, Eq. (8.315.1)] and [18, Eq. (1.60)] in sequence, it follows that

$$\mathrm{M}_X(t) = \prod_{j=1}^{2} \frac{z_j^2}{\alpha_j \Gamma(\mu_j)\Gamma(m_j)} \mathrm{H}_{5,4}^{4,3}\left[\frac{1}{(-t)} \prod_{j=1}^{2} \frac{\Psi_j^{1/\alpha_j}}{\hat{r}_j h_{l_j} A_{0_j}} \,\middle|\, \begin{matrix} (1,1), \mathcal{A}_1, \mathcal{A}_2, \mathcal{B}_1, \mathcal{B}_2 \\ \mathcal{C}_1, \mathcal{C}_2, \mathcal{D}_1, \mathcal{D}_2 \end{matrix} \right]. \tag{5.10}$$

Defining $R = \sum_{i=1}^{L} |h_{i,1}||h_{i,2}| = \sum_{i=1}^{L} \prod_{j=1}^{2} |h_{i,j}|$, it follows that $\mathrm{M}_R(t) = \prod_{i=1}^{L} \mathrm{M}_{X_i}(t)$. Using the definition of the multivariate Fox H-function [18, Eq. (A.1)], $\mathrm{M}_R(t)$ can be written as

$$\begin{aligned} \mathrm{M}_R(t) = & \left[\prod_{i=1}^{L} \prod_{j=1}^{2} \frac{z_{i,j}^2}{\alpha_{i,j}\Gamma(\mu_{i,j})\Gamma(m_{i,j})} \right] \\ & \times \mathrm{H}_{0,0:[5,4]_{i=1:L}}^{0,0:[4,3]_{i=1:L}} \left[\begin{matrix} \frac{\chi_1}{(-t)} \\ \vdots \\ \frac{\chi_L}{(-t)} \end{matrix} \,\middle|\, \begin{matrix} - \\ - \end{matrix} \,\middle|\, \begin{matrix} [(1,1), \mathcal{A}_{i,1}, \mathcal{A}_{i,2}, \mathcal{B}_{i,1}, \mathcal{B}_{i,2}]_{i=1:L} \\ [\mathcal{C}_{i,1}, \mathcal{C}_{i,2}, \mathcal{D}_{i,1}, \mathcal{D}_{i,2}]_{i=1:L} \end{matrix} \right], \end{aligned} \tag{5.11}$$

in which

$$\chi_i = \prod_{j=1}^{2} \frac{\Psi_{i,j}^{1/\alpha_{i,j}}}{\hat{r}_{i,j} h_{l_{i,j}} A_{0_{i,j}}}. \tag{5.12}$$

From (5.11), the PDF of R can be calculated as

$$f_R(r) = \frac{1}{2\pi j} \int_{\mathcal{C}} \mathrm{M}_R(t) \exp(st) dt \Big|_{(-r)}. \tag{5.13}$$

Using [16, Eq. (8.315.1)] and after algebraic simplifications,

$$\begin{aligned} f_R(r) = & \frac{1}{r} \left[\prod_{i=1}^{L} \prod_{j=1}^{2} \frac{z_{i,j}^2}{\alpha_{i,j}\Gamma(\mu_{i,j})\Gamma(m_{i,j})} \right] \\ & \times \mathrm{H}_{0,1:[5,4]_{i=1:L}}^{0,0:[4,3]_{i=1:L}} \left[\begin{matrix} \chi_1 r \\ \vdots \\ \chi_L r \end{matrix} \,\middle|\, \begin{matrix} - \\ \epsilon_1 \end{matrix} \,\middle|\, \begin{matrix} [(1,1), \mathcal{A}_{i,1}, \mathcal{A}_{i,2}, \mathcal{B}_{i,1}, \mathcal{B}_{i,2}]_{i=1:L} \\ [\mathcal{C}_{i,1}, \mathcal{C}_{i,2}, \mathcal{D}_{i,1}, \mathcal{D}_{i,2}]_{i=1:L} \end{matrix} \right]. \end{aligned} \tag{5.14}$$

Integrating (5.14),

$$F_R(r) = \left[\prod_{i=1}^{L}\prod_{j=1}^{2}\frac{z_{i,j}^2}{\alpha_{i,j}\Gamma(\mu_{i,j})\Gamma(m_{i,j})}\right] \times \mathrm{H}_{0,1:[5,4]_{i=1:L}}^{0,0:[4,3]_{i=1:L}}\left[\begin{array}{c|c|c} \chi_1 r & - & [(1,1),\mathcal{A}_{i,1},\mathcal{A}_{i,2},\mathcal{B}_{i,1},\mathcal{B}_{i,2}]_{i=1:L} \\ \vdots & \epsilon_5 & [\mathcal{C}_{i,1},\mathcal{C}_{i,2},\mathcal{D}_{i,1},\mathcal{D}_{i,2}]_{i=1:L} \\ \chi_L r & & \end{array}\right], \tag{5.15}$$

with $\epsilon_5 = (0;\{1\}_{i=1:L})$.

Making $\Gamma = R^2$, the PDF of the instantaneous SNR can be obtained using (3.8), as shown in (5.2). Integrating (5.2), knowing that $\int_0^\gamma x^{n-1}\mathrm{d}x = \gamma^n/n$, $\Gamma(\gamma+1) = \gamma\Gamma(\gamma)$ and using the definition of the multivariate H-Fox, (5.3) is obtained. Finally, the MGF is deduced by computing the Laplace transform of (5.2). Using [14, id 01.03.26.0004.01], [14, id 07.34.26.0008.01], [18, Eq. (2.8)] and [18, Eq. (A.1)], (5.4) is derived. Hence, the proof is concluded. □

It should be mentioned that the statistics presented in this chapter are equal to [8], with $m_s \to \infty$, and equal to [26], for $z \to \infty$. Thus, our work generalizes some results presented in [8, 26]. Furthermore, it should be highlighted that the envelope statistics presented in the proof are also contributions of this work.

5.3 PERFORMANCE ANALYSIS

5.3.1 Outage Probability

The OP is given by $P_{\mathrm{out}} = F_\Gamma(\gamma_{\mathrm{th}})$, in which $F_\Gamma(\cdot)$ is written as (5.3).

5.3.2 Bit Error Probability

The average bit error probability (BEP), P_{b}, can be evaluated as [27]

$$P_{\mathrm{b}} = \frac{1}{\pi}\int_0^{\frac{\pi}{2}} \mathrm{M}_\Gamma\left(\frac{\rho}{\sin^2\theta}\right)\mathrm{d}\theta, \tag{5.16}$$

in which ρ depends on the type of modulation considered.

Substituting (5.4) in (5.16), employing [18, Eq. (A.1)] and performing the change of variable $x = \sin^2\theta$, and using [16, Eq. (3.191.3)/Eq. (8.384.1)] in sequence, it follows that the BEP can be written in

closed-form, after simplifications, as

$$P_{\rm b} = \frac{1}{4\sqrt{\pi}} \left[\prod_{i=1}^{L} \prod_{j=1}^{2} \frac{z_{i,j}^2}{\alpha_{i,j}\Gamma(\mu_{i,j})\Gamma(m_{i,j})} \right] \times \mathrm{H}_{2,2:[5,4]_{i=1:L}}^{0,2:[4,3]_{i=1:L}} \left[\begin{array}{c|c|c} \frac{\Xi_1}{\sqrt{\rho}} & & \\ \vdots & \epsilon_3, \epsilon_4 & [(1,1), \mathcal{A}_{i,1}, \mathcal{A}_{i,2}, \mathcal{B}_{i,1}, \mathcal{B}_{i,2}]_{i=1:L} \\ \frac{\Xi_L}{\sqrt{\rho}} & \epsilon_1, \epsilon_2 & [\mathcal{C}_{i,1}, \mathcal{C}_{i,2}, \mathcal{D}_{i,1}, \mathcal{D}_{i,2}]_{i=1:L} \end{array} \right], \tag{5.17}$$

with $\epsilon_4 = \left(\frac{1}{2}; \{\frac{1}{2}\}_{i=1:L}\right)$.

5.4 ASYMPTOTIC ANALYSIS

From (5.3) and (5.17) respectively, and considering the approach presented in [28], it follows that the asymptotic OP and BEP expressions can be written as

$$P_{\rm out}^{\infty} = \frac{1}{2\mathcal{B}} \left[\prod_{i=1}^{L} \prod_{j=1}^{2} \frac{z_{i,j}^2}{\alpha_{i,j}\Gamma(\mu_{i,j})\Gamma(m_{i,j})} \right] \Psi(U_1, ..., U_L) \prod_{i=1}^{L} \phi(U_i) \left(\Xi_i \gamma_{\rm th}^{\frac{1}{2}} \right)^{U_i} \tag{5.18}$$

and

$$P_{\rm b}^{\infty} = \frac{1}{4\sqrt{\pi}\mathcal{B}} \left[\prod_{i=1}^{L} \prod_{j=1}^{2} \frac{z_{i,j}^2}{\alpha_{i,j}\Gamma(\mu_{i,j})\Gamma(m_{i,j})} \right] \Psi(U_1, ..., U_L) \prod_{i=1}^{L} \phi(U_i) \left(\Xi_i \rho^{-\frac{1}{2}} \right)^{U_i}, \tag{5.19}$$

in which $\mathcal{B} = \prod_{i=1}^{L} B_{i,c_i}$,

$$U_i = \min_{1 \le j \le 4} \left\{ \mu_{i,1}\alpha_{i,1}, \mu_{i,2}\alpha_{i,2}, z_{i,1}^2, z_{i,2}^2 \right\}, \tag{5.20}$$

$$c_i = \arg \min_{1 \le j \le 4} \left\{ \mu_{i,1}\alpha_{i,1}, \mu_{i,2}\alpha_{i,2}, z_{i,1}^2, z_{i,2}^2 \right\}, \tag{5.21}$$

$$\phi(U_i) = \frac{\displaystyle\prod_{j=1,\ \mu_{i,j} \neq \frac{U_i}{\alpha_{i,j}}}^{2} \Gamma\left(\mu_{i,j} - \frac{U_i}{\alpha_{i,j}}\right) \prod_{j=1,\ z_{i,j}^2 \neq U_i}^{2} \Gamma\left(\frac{z_{i,j}^2}{\alpha_{i,j}} - \frac{U_i}{\alpha_{i,j}}\right) \prod_{j=1}^{2} \Gamma\left(m_{i,j} + \frac{U_i}{\alpha_{i,j}}\right) \Gamma(U_i)}{\displaystyle\prod_{j=1}^{2} \Gamma\left(\frac{z_{i,j}^2}{\alpha_{i,j}} + 1 - \frac{U_i}{\alpha_{i,j}}\right)}, \tag{5.22}$$

$$\Psi(U_1,...,U_L)=\frac{\Gamma\left(\sum_{i=1}^{L}\frac{1}{2}U_i\right)}{\Gamma\left(\sum_{i=1}^{L}U_i\right)\Gamma\left(1+\sum_{i=1}^{L}\frac{1}{2}U_i\right)} \tag{5.23}$$

for the OP and

$$\Psi(U_1,...,U_L)=\frac{\Gamma\left(\sum_{i=1}^{L}\frac{1}{2}U_i\right)\Gamma\left(\frac{1}{2}+\sum_{i=1}^{L}\frac{1}{2}U_i\right)}{\Gamma\left(\sum_{i=1}^{L}U_i\right)\Gamma\left(1+\sum_{i=1}^{L}\frac{1}{2}U_i\right)} \tag{5.24}$$

for the BEP. It should be mentioned that the diversity order is given by

$$G_{\mathrm{d}}=\sum_{i=1}^{L}\min_{1\leq j\leq 4}\left\{\mu_{i,1}\alpha_{i,1},\mu_{i,2}\alpha_{i,2},z_{i,1}^2,z_{i,2}^2\right\}. \tag{5.25}$$

6 RESULTS

Theoretical curves as a function of the average SNR $\bar{\gamma}$ are shown in Fig. 6.1, corroborated by Monte-Carlo simulations, under different values of the parameter z in order to characterize scenarios with weak, moderate, and heavy pointing errors. In our simulations, the Fox H-function implementation available in [29] is considered. In addition, $A_0 = 0.8$ and without loss of generality, $h_{\rm l} = 1$. In all cases, the adherence between the theoretical and simulated curves is perceived. Also, the asymptotic curves follow the analytical ones at high SNR.

The SEP is evaluated in Fig. 6.1(a), with $\alpha = 3.5$, $m = 5$, and $\mu = 2$, for BPSK and QPSK modulation schemes. The asymptotic curves are plotted from (4.7). As z increases, it is noted that the SEP decreases since the pointing error condition is improving. For $\bar{\gamma} = 10$ dB, a gain in terms of SEP of approximately two orders of magnitude is perceived when comparing the curves for the case where the BPSK scheme is adopted, with weak ($z = 6.5$) and heavy ($z = 0.6$) pointing error scenarios. For z fixed, the SEP is better for the BPSK scheme than the one for QPSK, as the receiver is less likely to make errors in the decision process. Fig. 6.1(b) presents OP curves under different values of α, for $\mu = 2.7$, $m = 1.3$ and $\gamma_{\rm th} = 5$ dB. Asymptotic curves are plotted with (4.5). For $\alpha = 2$, the Fisher-Snedecor case is provided as a benchmark. As the parameter α increases the OP improves for a given z value. The following insight is also perceived in Fig. 6.1(b): for the strong pointing errors case, the increase in the value of α has almost no impact on the OP. Capacity and asymptotic capacity curves as a function of SNR are plotted in Fig. 6.1(c), under different m values, with $\alpha = 2.2$ and $\mu = 2.1$. In our analysis, $m = 3.1$ and $m = 10.5$ denote moderate and weak shadowing, respectively. Lower capacity values are obtained for $z = 0.6$, which corresponds to a scenario with heavy pointing errors. Furthermore, for weak, moderate, or heavy pointing errors, smaller capacity values are also obtained for $m = 3.1$.

Fig. 6.2 presents SEP curves as a function of SNR $\bar{\gamma}$, considering the BPSK modulation scheme, $z = 3$, $m = \{2.5, \infty\}$, $\alpha = \{2, 6.5\}$ and $\mu = \{1, 1.7\}$. In our model, the α-μ with misalignment is obtained when $m \to \infty$. In turn, for $\alpha = 2$, the Fisher-Snedecor $\mathcal{F}$ distribution with pointing errors is achieved. For $\mu = 1$, the shadowed Weibull fading model also with the mentioned effect can be obtained as a particular case of the study proposed in this work. To the best of the authors' knowledge, results for the shadowed Weibull model with pointing errors have not been presented in the literature. In Fig. 6.2, it is evidenced that (i) for a fixed SNR, the SEP increases as the parameter that characterizes the shadowing (m) effect and/or the parameter that models the fading intensity decreases and (ii) the impact of the m and μ on the SEP is smaller as α increases.

Comparisons between the empirical and theoretical PDFs of the α-μ and α-$\mathcal{F}$ distributions are performed in Fig. 6.3. The empirical data were extracted from [10, Fig. 2(c)] using the WebPlotDigitizer tool and the parameters of the theoretical PDFs were estimated using the lsqcurvefit function available in Matlab. For the α-μ distribution, it should be mentioned that the estimated parameters are the same as found in [10, Table 5, TX4]. It is noted in Fig. 6.3 that the α-$\mathcal{F}$ model presents practically the same adherence as the α-μ distribution, as expected, since the measured data did not consider shadowing. For this scenario, the α-$\mathcal{F}$ is slightly better than α-μ distribution in terms of MSE and has a large m value, which is expected

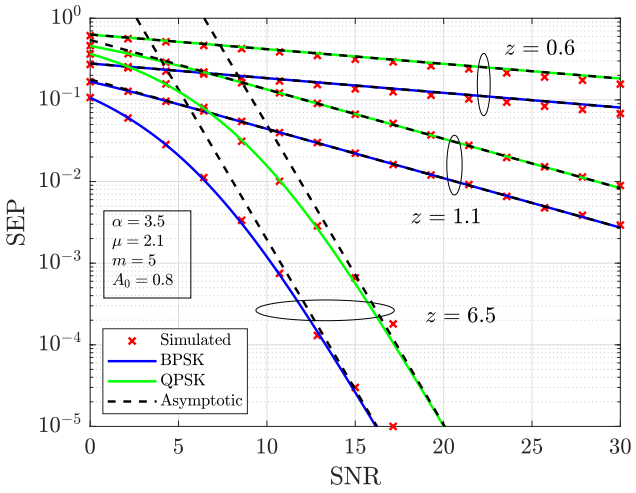

(a)

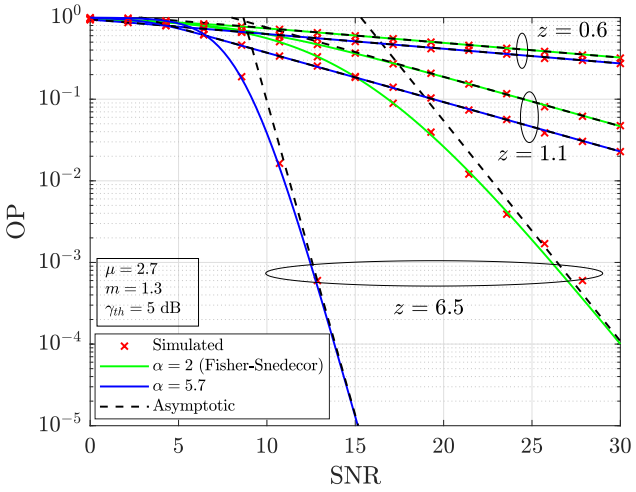

(b)

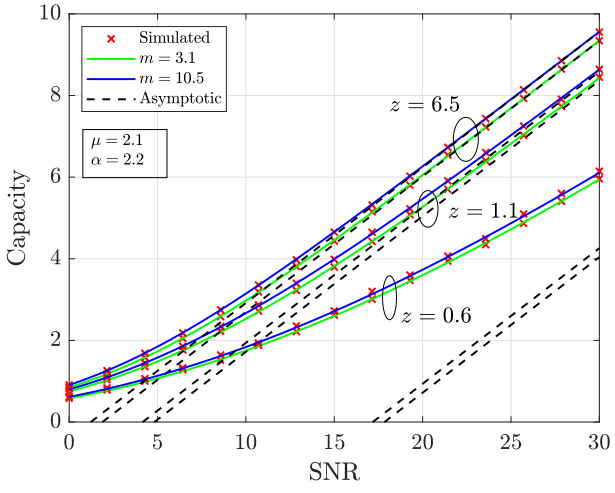

(c)

Figure 6.1: (a) SEP, (b) OP, and (c) capacity curves as a function of SNR $\bar{\gamma}$, considering weak, moderate, and heavy pointing errors.

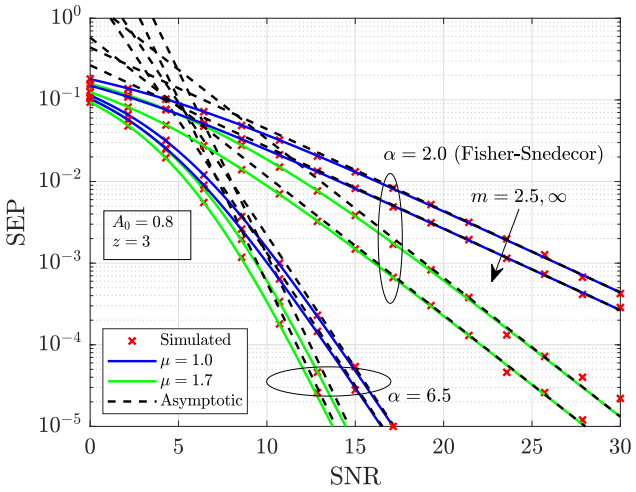

Figure 6.2: SEP curves as a function of SNR $\bar{\gamma}$, considering the BPSK modulation.

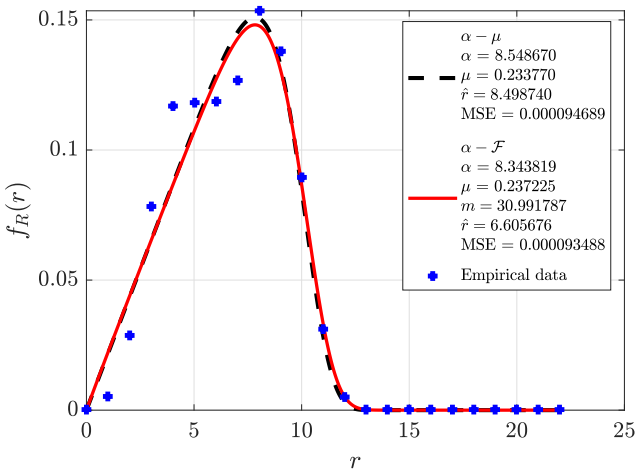

Figure 6.3: Comparisons between the empirical and the theoretical PDFs.

in a non-shadowing scenario. This supports the mathematical framework developed and the model itself. For the case in which shadowing can be considered, it is expected that the α-$\mathcal{F}$ distribution presents a better adherence than the α-μ since the mentioned distribution has a higher degree of freedom. This indicates the promising potential of employing the α-$\mathcal{F}$ distribution to model THz channels.

The OP and the BEP curves are presented in Figs. 6.4(a) and (b), respectively, under RIS-assisted scenarios considering α-$\mathcal{F}$ fading with pointing errors. In our study, independent and non-identically distributed variates are adopted. In Fig. 6.4(a), $\alpha_{i,1} = 1.5$, $\alpha_{i,2} = 2.3$, $\mu_{i,1} = \mu_{i,2} = 2.0$, $m_{i,1} = 3.0$, $m_{i,2} = 4.0$, $z_{i,1} = 0.8$, $z_{i,2} = 1.5$ and $\gamma_{\text{th}} = 5$ dB. In Fig. 6.4(b), $\alpha_{i,1} = 1.5$, $\alpha_{i,2} = 2.3$, $\mu_{i,1} = 2.5$, $\mu_{i,2} = 3.5$, $m_{i,1} = 4.0$, $m_{i,2} = 5.0$, $z_{i,1} = 0.8$, $z_{i,2} = 1.5$ and $\rho = 1$. The curves in Fig. 6.4 are shown as a function of SNR, for different number of the RIS elements, under strong and moderate pointing errors. Asymptotic curves are also plotted with (5.18) and (5.19). In Fig. 6.4, the impact of the RIS elements on the metrics performance is evidenced. From our results, it is noted that the RIS improves the OP and BEP performance, consonant with (5.25). In fact, as L increases lower is the OP and BEP values obtained.

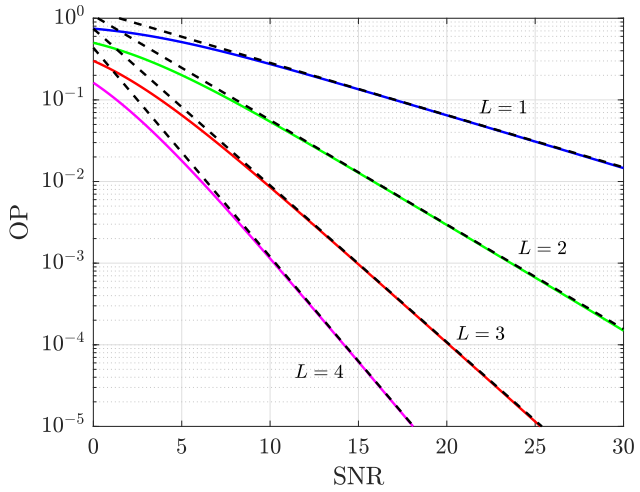

(a)

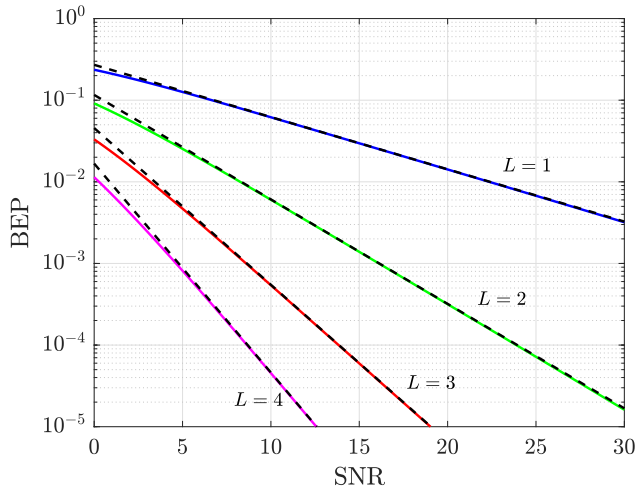

(b)

Figure 6.4: (a) OP and (b) BEP curves as a function of SNR $\bar{\gamma}$, under RIS-assisted scenarios considering α-$\mathcal{F}$ fading with pointing errors. Theoretical expressions are the solid curves and the asymptotic are the tracejed.

Furthermore, as evidenced in (5.25), it should be mentioned that the diversity gain depends on the fading and pointing errors parameters and thus, note that the slope of the curves change according to the mentioned parameters.

7 CONCLUSIONS

This study advanced the knowledge of α-$\mathcal{F}$ fading model by considering the pointing errors impairment. Important statistics, such as the PDFs and the CDFs, higher-order moments, and moment generating function of the instantaneous SNR were derived, as well as the outage probability, symbol error probability, and ergodic channel capacity metrics. Curves were presented for the mentioned metrics and validated using Monte-Carlo simulations. In all scenarios studied, a strong adherence between the theoretical and simulated curves was noticed, which validates our analysis. In addition, an application of the α-$\mathcal{F}$ distribution with pointing errors was performed in a wireless emerging system, namely reconfigurable intelligent surfaces, thus evidencing the usefulness and capability of our model in practical scenarios.

Appendix

APPENDIX A

The Fox H-function can be written in terms of the Mellin-Barnes integral, that is a contour integral involving a product of gamma functions; and is given by

$$\mathrm{H}_{p,q}^{m,n}\left[z\left|\begin{array}{c}(a_1,A_1),(a_2,A_2),\cdots,(a_p,A_p)\\(b_1,B_1),(b_2,B_2),\cdots,(b_q,B_q)\end{array}\right.\right] = \frac{1}{2\pi w}\int_L \frac{\prod_{j=1}^{m}\Gamma\left(b_j+B_j s\right)\prod_{j=1}^{n}\Gamma\left(1-a_j-A_j s\right)}{\prod_{j=n+1}^{p}\Gamma\left(a_j+A_j s\right)\prod_{j=m+1}^{q}\Gamma\left(1-b_j-B_j s\right)} z^{-s} ds. \tag{7.1}$$

In (7.1), w is imaginary unit.

APPENDIX B

The Meijer G-function is a particular case of the Fox H function, in which the second pair of elements is equal to 1, that is, $A_j = 1$, $B_j = 1$ and can be represented by

$$\mathrm{G}_{p,q}^{m,n}\left[z\left|\begin{array}{c}a_1,a_2,\cdots,a_p\\b_1,b_2,\cdots,b_q\end{array}\right.\right] = \frac{1}{2\pi w}\int_L \frac{\prod_{j=1}^{m}\Gamma\left(b_j+s\right)\prod_{j=1}^{n}\Gamma\left(1-a_j-s\right)}{\prod_{j=n+1}^{p}\Gamma\left(a_j+s\right)\prod_{j=m+1}^{q}\Gamma\left(1-b_j-s\right)} z^{-s} ds, \tag{7.2}$$

in witch w is imaginary unit.

APPENDIX C

The multivariable H-function can be defined by multiples Mellin-Barnes type contour integral as

$$\mathrm{H}_{p,q:p_1,q_1;\ldots;p_r,q_r}^{0,n:m_1,n_1;\ldots;m_r,n_r}\left[\begin{array}{c}z_1\\\vdots\\z_r\end{array}\left|\begin{array}{c|c|c}(a_j;A_j^{(1)},\cdots,A_j^{(r)})_{j=1:p} & (c_j^{(1)},C_j^{(1)})_{j=1:p_1});\cdots;(c_j^{(r)},C_j^{(r)})_{j=1:p_r)}\\(b_j;B_j^{(1)},\cdots,B_j^{(r)})_{j=1:q} & (d_j^{(1)},D_j^{(1)})_{j=1:q_1});\cdots;(d_j^{(r)},D_j^{(r)})_{j=1:q_r)}\end{array}\right.\right]$$
$$= \frac{1}{(2\pi w)^r}\int_{L_1}\cdots\int_{L_r}\Psi(\zeta_1,\ldots,\zeta_r)\left\{\prod_{i=1}^{r}\phi_i(\zeta_i)z_i^{\zeta_i}\right\}d\zeta_1\cdots d\zeta_r, \tag{7.3}$$

in witch w is imaginary unit and

$$\Psi(\zeta_1,\ldots,\zeta_r) = \frac{\prod_{j=1}^{n}\Gamma(1-a_j+\sum_{i=1}^{r}A_j^{(i)}\zeta_j)}{\left[\prod_{j=n+1}^{p}\Gamma(a_j-\sum_{i=1}^{r}A_j^{(i)}\zeta_j)\right]\left[\prod_{j=1}^{q}\Gamma(1-b_j+\sum_{i=1}^{r}B_j^{(i)}\zeta_j)\right]}, \tag{7.4}$$

$$\phi_j(\zeta_j) = \frac{\prod_{j=1}^{m_j} \Gamma(d_j^{(i)} - D_j^{(i)}\zeta_j) \prod_{j=1}^{n_i} \Gamma(1 - c_j^{(i)} + C_j^{(i)}\zeta_i)}{\prod_{j=n+1}^{p_i} \Gamma(c_j^{(i)} - C_j^{(i)}\zeta_i) \prod_{j=m+1}^{q_i} \Gamma(1 - d_j^{(i)} + D_j^{(i)}\zeta_i)}. \tag{7.5}$$

BIBLIOGRAPHIC REFERENCES

1 HAN, C.; WANG, Y.; LI, Y.; CHEN, Y.; ABBASI, N. A.; KüRNER, T.; MOLISCH, A. F. Terahertz wireless channels: A holistic survey on measurement, modeling, and analysis. arXiv:2111.04522v2, 2022.

2 BOULOGEORGOS, A. A.; PAPASOTIRIOU, E. N.; ALEXIOU, A. Analytical performance assessment of thz wireless systems. *IEEE Access*, vol. 7, pp. 11436-11453, 2019.

3 BADARNEH, O. S. Performance analysis of terahertz communications in random fog conditions with misalignment. *IEEE Wirel. Commun. Lett.*, vol. 11, no. 5, 962-966, 2022.

4 SAI, S.; YANG, L. Performance analysis of dual-hop THz transmission systems over α-μ fading channels with pointing errors. *IEEE Internet Things J.*, vol. 9, no. 14, pp. 11772-11783, 2022.

5 CANG, L. Terahertz MIMO communication performance analysis in exponentiated Weibull turbulence with pointing errors. *IEEE Commun. Lett.*, vol. 26, no. 7, pp. 1678-1682, 2021.

6 DING, Z.; POOR, H. V. Design of THz-NOMA in the presence of beam misalignment. *Appl. Opt.*, vol. 60, no. 24, pp. 7314-7325, 2022.

7 BADARNEH, O. S. Performance analysis of FSO communications over $\mathcal{F}$ turbulence channels with pointing errors. *IEEE Commun. Lett.*, vol. 25, no. 3, pp. 926-930, 2021.

8 CHAPALA, V. K.; ZAFARUDDIN, S. M. Exact analysis of RIS-aided THz wireless systems over α-μ fading with pointing errors. *IEEE Commun. Lett.*, vol. 9, no. 14, pp. 3508-3512, 2022.

9 BOULOGEORGOS, A. A.; RIERA, J. M.; ALEXIOU, A. On the joint effect of rain and beam misalignment in terahertz wireless systems. *IEEE Access*, vol. 10, pp. 58997-59012, 2022.

10 PAPASOTIRIOU, E. N. An experimentally validated fading model for THz wireless systems. *Scientific Reports*, vol. 11, no. 18717, pp. 1-14, 2021.

11 PAPASOTIRIOU, E. N. A new look to THz wireless links: Fading modeling and capacity assessment. in Proc. of *IEEE International Symposium on Personal, Indoor and Mobile Radio Communications*, pp. 1-5, 2021.

12 YE, J. On outage performance of terahertz wireless communication systems. *IEEE Trans. Commun.*, vol. 70, no. 1, pp. 649-663, 2022.

13 BADARNEH, O. S. The α-$\mathcal{F}$ composite fading distribution: Statistical characterization and applications. *IEEE Trans. Veh. Technol.*, vol. 69, no. 8, pp. 8097-8106, 2020.

14 RESEARCH, I. W. Available: http://functions.wolfram.com/id. *Wolfram Research.*, 2020.

15 ANSARI, I. S.; YILMAZ, F.; ALOUINI, M. S. Performance analysis of free-space optical links over málaga ($\mathcal{M}$) turbulence channels with pointing errors. *IEEE Trans. Wirel. Commun.*, vol. 15, no. 1, pp. 91-102, 2016.

16 GRADSHTEYN, I. S.; RYZHIK, I. M. Table of integrals, series and products. New York: Academic Express, 2007.

17 PRUDNIKOV, A. P.; BRYCHKOV, Y. A.; MARICHEV, O. I. Integral and series: Volume 3, more special functions. Florida: CRC, Press Inc., 1990.

18 MATHAI, A. M.; SAXENA, R. K.; HAUBOLD, H. J. The H-function: Theory and applications. New York, NY, USA: Springer, 2009.

19 KILBAS, A. A.; SAIGO, M. *H-Transforms: Theory and Applications*. Florida: CRC Press Inc, 2004.

20 BADARNEH, O. S.; MUHAIDAT, S.; COSTA, D. B. da. The α-η-κ-$\mathcal{F}$ composite fading distribution. *IEEE Wirel. Commun. Lett.*, vol. 9, no. 12, pp. 2182-2186, 2020.

21 YILMAZ, F.; ALOUINI, M. S. Novel asymptotic results on the high-order statistics of the channel capacity over generalized fading channels. in Proc. of *IEEE SPAWC*, pp. 389-393, 2012.

22 WEI, L.; HUANG, C.; ALEXANDROPOULOS, G. C.; YUEN, C.; ZHANG, Z.; DEBBAH, M. Channel estimation for RIS- empowered multi-user MISO wireless communications. *IEEE Trans. Commun.*, vol. 69, no. 6, pp. 4144–4157, 2021.

23 WU, Q.; ZHANG, R. Towards smart and reconfigurable environment: Intelligent reflecting surface aided wireless network. *IEEE Commun. Mag.*, vol. 58, no. 1, pp. 106–112, 2020.

24 XU, Y.; CHU, H.; XU, P. Joint channel estimation and passive beamforming for reconfigurable intelligent surface aided multi-user massive mimo system. in Proc. of IEEE BlackSeaCom, pp. 1-3, 2021.

25 SPRINGER, M. D.; THOMPSON, W. E. The distribution of products of independent random variables. *SIAM J. Appl. Math.*, vol. 14, no. 3, pp. 511-526, 1966.

26 SILVA, H. S.; et al. On the sum of α-$\mathcal{F}$ and double α-$\mathcal{F}$ variates with application to MRC and RIS. *IEEE Commun. Lett.*, vol. 26, no. 12, pp. 2894-2898, 2022.

27 PROAKIS, J. G.; SALEHI, M. Digital communications. *New York: McGraw-Hill*, 2008.

28 RAHAMA, Y. A.; ISMAIL, M. H.; HASSAN, M. S. On the sum of independent fox's h-function variates with applications. *IEEE Trans. Veh. Technol.*, vol. 67, no. 8, pp. 6752-6760, 2018.

29 SOULIMANIA, A.; BENJILLALIA, M.; CHERGUI, H.; COSTA, D. B. da. Multihop Weibull-fading communications: performance analysis framework and applications. *J. Franklin Inst.*, vol. 358, no. 15, pp. 1-35, 2021.